Microscopic core-quasiparticle coupling model for spectroscopy of odd-mass nuclei with octupole correlations

W. Sun,[1] S. Quan,[1] Z. P. Li [●],[1,2,*] J. Zhao [●],[3] T. Nikšić,[4] and D. Vretenar[4]

[1]*School of Physical Science and Technology, Southwest University, Chongqing 400715, China*
[2]*Department of Physics and Electronic Science, Qiannan Normal University for Nationalities, Duyun 558000, China*
[3]*Microsystem and Terahertz Research Center and Insititute of Electronic Engineering,*
China Academy of Engineering Physics, Chengdu 610200, Sichuan, China
[4]*Physics Department, Faculty of Science, University of Zagreb, Bijenička Cesta 32, Zagreb 10000, Croatia*

Background: Predictions of spectroscopic properties of low-lying states are critical for nuclear structure studies. Theoretical methods can be particularly involved for odd-mass nuclei because of the interplay between the unpaired nucleon and collective degrees of freedom. Only a few models have been developed for systems in which octupole collective degrees of freedom play a role.

Purpose: We aim to predict spectroscopic properties of odd-mass nuclei characterized by octupole shape deformation, employing a model that describes single-particle and collective degrees of freedom within the same microscopic framework.

Method: A microscopic core-quasiparticle coupling (CQC) model based on the covariant density functional theory is developed, which includes collective excitations of even-mass core nuclei and single-particle states of the odd nucleon, calculated using a quadrupole-octupole collective Hamiltonian combined with a constrained reflection-asymmetric relativistic Hartree-Bogoliubov model.

Results: Model predictions for low-energy excitation spectra and transition rates of odd-mass radium isotopes ^{223,225,227}Ra are shown to be in good agreement with available data.

Conclusions: A microscopic CQC model based on covariant density functional theory has been developed for odd-mass nuclei characterized by both quadrupole and octupole shape deformations. Theoretical results reproduce data in odd-mass Ra isotopes and provide useful predictions for future studies of octupole correlations in nuclei and related phenomena.

I. INTRODUCTION

Studies of reflection-asymmetric octupole shapes have been a recurrent theme of interest in nuclear structure physics over several decades. More recently, experimental evidence for stable octupole deformation in nuclei has been reported, e.g., in ^{224}Ra [1], ^{144}Ba [2], and ^{146}Ba [3]. This type of shape deformation occurs predominantly in nuclei with neutron (proton) number $N(Z) \approx 34$, 56, 88, and 134, characterized by the presence of low-lying negative-parity bands as well as pronounced electric octupole transitions [4,5].

Octupole deformation in nuclei with an odd nucleon number has attracted specific interest in connection with observed parity-doublet structures and enhanced Schiff moments [4,6–8]. In the last decade considerable effort has been devoted to studies of excited states in odd-mass nuclei characterized by static and dynamic octupole deformation [9–21]. New levels, transitions, and/or dipole moments have been measured for nuclei in different mass regions, e.g., neutron-rich nuclei around ^{144}Ba [9–15], neutron-deficient nuclei approaching $N, Z \approx 56$ [16,17], heavy nuclei around ^{224}Ra

[18–21]. Furthermore, it is expected that heavy odd-mass octupole-deformed nuclei, such as ^{225}Ra, amplify atomic electric dipole moments (EDMs) and related nuclear Schiff moments that arise from time-reversal and parity-violating interactions in the nuclear medium [22–26]. Effects of symmetry violation are greatly enhanced in ^{225}Ra by collective effects and a closely spaced parity-doublet structure resulting from octupole nuclear deformation [23,25]. As a wealth of new data on odd-*A* systems become accessible, it is important to develop consistent and accurate models that can be employed in theoretical studies of their spectroscopic properties.

A variety of theoretical methods have been applied to studies of octupole nuclear shapes and the evolution of the corresponding negative-parity collective states: self-consistent mean-field approaches [27–56], macroscopic + microscopic (MM) models [57–59], algebraic (or interacting boson) models [60,61], phenomenological collective models [62–67], and the reflection asymmetric shell model [68]. For the case of odd-*A* nuclei theoretical approaches include the particle-rotor model [69–75], the cluster model [76], the reflection-asymmetric shell model [77], the interacting boson-fermion model [78], etc. Microscopic calculations for odd-mass nuclei are generally more complex because, in addition to collective degrees of freedom, one has to explicitly consider

---
*[*]zpliphy@swu.edu.cn

single-particle degrees of freedom. To this end, nuclear energy density functionals (EDFs) generally present a good starting point since EDFs enable a complete and accurate description of ground-state properties, collective excitations, and decay properties over the entire chart of nuclides [79–92]. Recently several EDF-based approaches, e.g., the generator coordinate method (GCM) built on blocked one-quasiparticle states [93–95], the interacting boson-fermion model (IBFM) [96], and the core-quasiparticle coupling (CQC) model [97] have been implemented for spectroscopic studies of odd-*A* quadrupole-deformed nuclei. Microscopic models for odd-A nuclei with octupole deformation are much less developed. Only very recently the IBFM was extended to include both quadrupole and octupole boson degrees of freedom and applied to a study of low-lying positive- and negative-parity spectra of odd-*A* $^{143-147}$Ba [30].

In this work we extend the microscopic core-quasiparticle coupling model of Ref. [97] to include both quadrupole and octupole deformations in reflection-asymmetric odd-mass nuclear systems, based on the framework of covariant EDFs [80,84]. The major development is the inclusion of octupole correlations in both the even-even core Hamiltonian [50–52,98], with parameters determined by the axially reflection-asymmetric relativistic Hartree-Bogoliubov model calculations, and the core-quasiparticle coupling terms. Also, the inclusion of both neighboring even-even cores in the configuration space enables the model to take into account shape polarization effects, that is, differences in shapes and related observables which are critical for transitional nuclei [99]. The present study is focused on the low-lying positive- and negative-parity spectra of odd-*A* ^{223,225,227}Ra, located in the vicinity of the even-even nucleus ^{224}Ra with static octupole deformation. Furthermore, ^{225}Ra is a favorable case to search for a permanent electric dipole moment.

In Sec. II the model and self-consistent microscopic calculation of the parameters of the Hamiltonian are described. Illustrative results for spectroscopic properties, such as low-lying excitation spectra, electric transitions, and wave functions are discussed in Sec. III. Section IV contains a summary of the principal results.

II. THEORETICAL FRAMEWORK

A. Core-quasiparticle coupling model with quadrupole and octupole interactions

In the core-quasiparticle coupling scheme, the configuration space of the odd-*A* nucleus is composed of both a particle coupled to the lighter even-even neighbor $A - 1$ and a hole coupled to the heavier even-even neighbor $A + 1$. For an odd-*A* nucleus in which low-energy excitation spectra are determined by octupole correlations, both the ground-state bands and the lowest negative-parity bands of the even-even cores are included in the configuration space. The ansatz for the wave function of the odd-mass system can therefore be written in the following form:

$$|\alpha J M_J \pi\rangle^A = \sum_{\mu\Omega} \left\{ U_{\mu\Omega} [a_\mu^\dagger |\Omega\rangle]_{JM_J\pi}^{A-1} + V_{\mu\Omega} [a_\mu |\Omega\rangle]_{JM_J\pi}^{A+1} \right\},$$

(1)

where the total angular momentum is J, its projection is M_J, π denotes the parity, and α denotes all additional quantum numbers that characterize the state. μ denotes the angular momentum j, its projection m_j, parity π_j, and additional quantum numbers n_μ of single-particle states, while Ω is the generic notation for the angular momentum R, its projection M_R, parity π_R, and additional quantum numbers n_Ω of collective states of the even-even core. The coefficients $U_{\mu\Omega}$ and $V_{\mu\Omega}$ represent the probability amplitudes for the particle-like and hole-like states, respectively, that are formed by coupling the spherical single-particle state $|\mu\rangle^{A-1}$ to the collective state $|\Omega\rangle^{A-1}$ of the core $A - 1$, and the spherical single-hole state $|\mu\rangle^{A+1}$ to the corresponding collective state $|\Omega\rangle^{A+1}$ of the core $A + 1$.

The Hamiltonian of the CQC model reads

$$H = H_{\rm qp} + H_{\rm c}$$
$$= \begin{pmatrix} (\varepsilon^{A-1} - \varepsilon_f) + \Gamma^{A-1} & \Delta^{A+1} \\ \Delta^{\dagger A-1} & -(\varepsilon^{A+1} - \varepsilon_f) - \Gamma^{A+1} \end{pmatrix}$$
$$+ \begin{pmatrix} E^{A-1} & 0 \\ 0 & E^{A+1} \end{pmatrix}.$$

(2)

The matrices $(\varepsilon^{A\pm1} - \varepsilon_f)$ and $(E^{A\pm1})$ are diagonal with respect to the basis states in the decomposition (1):

$$(\varepsilon^{A\pm1} - \varepsilon_f) = (\varepsilon_\mu^{A\pm1} - \varepsilon_f)\delta_{\mu\mu'}\delta_{\Omega\Omega'},$$

(3)

$$(E^{A\pm1}) = E_\Omega^{A\pm1}\delta_{\mu\mu'}\delta_{\Omega\Omega'}$$

(4)

with the spherical single-particle energies $\varepsilon_\mu^{A\pm1}$, Fermi surface ε_f, and collective excitation energies $E_\Omega^{A\pm1}$. Γ and Δ denote the mean field and pairing field that correspond to the long-range particle-hole and short-range particle-particle interactions, respectively. The quadrupole-quadrupole and octupole-octupole interactions determine the fields Γ, and a monopole pairing force is used for Δ:

$$(\Gamma^{A\pm1}) = -\chi_2(-1)^{j+R+J} \begin{Bmatrix} j & 2 & j' \\ R' & J & R \end{Bmatrix}$$
$$\times [\langle\mu\|\hat{Q}_2\|\mu'\rangle\langle\Omega\|\hat{Q}_2\|\Omega'\rangle]^{A\pm1}$$
$$- \chi_3(-1)^{j+R+J} \begin{Bmatrix} j & 3 & j' \\ R' & J & R \end{Bmatrix}$$
$$\times [\langle\mu\|\hat{Q}_3\|\mu'\rangle\langle\Omega\|\hat{Q}_3\|\Omega'\rangle]^{A\pm1},$$

(5)

$$(\Delta^{A+1}) = (\Delta^{A-1}) = \langle\Omega, A-1|\hat{\Delta}|\Omega', A+1\rangle\delta_{\mu\mu'}$$
$$\approx \frac{1}{2}(\Delta_\Omega^{A-1} + \Delta_\Omega^{A+1})\delta_{\mu\mu'}\delta_{\Omega\Omega'} \equiv (\Delta),$$

(6)

where $\langle\mu\|\hat{Q}_\lambda\|\mu'\rangle^{A\pm1}$ and $\langle\Omega\|\hat{Q}_\lambda\|\Omega'\rangle^{A\pm1}$ are the reduced quadrupole ($\lambda = 2$) and octupole ($\lambda = 3$) matrix elements of the spherical single-nucleon and core states, respectively. χ_2 and χ_3 are the corresponding coupling strengths of the quadrupole and octupole fields. $\Delta_\Omega^{A\pm1}$ denotes the average pairing fields in the collective states $|\Omega\rangle^{A\pm1}$.

The Fermi surface ε_f and coupling strengths χ_2 and χ_3 are free parameters that are adjusted to reproduce the

experimental ground-state spin and parity and/or the excitation energies of few lowest levels. Finally, the excitation

energies $E_{\alpha J \pi}$ and eigenvectors $U_{\mu\Omega}$, $V_{\mu\Omega}$ are obtained as solutions of the eigenequation

$$
\begin{pmatrix} (\varepsilon^{A-1} - \varepsilon_f) + \Gamma^{A-1} + E^{A-1} & \Delta \\ \Delta & -(\varepsilon^{A+1} - \varepsilon_f) - \Gamma^{A+1} + E^{A+1} \end{pmatrix} \begin{pmatrix} U \\ V \end{pmatrix} = E_{\alpha J \pi} \begin{pmatrix} U \\ V \end{pmatrix} \tag{7}
$$

following the method introduced in Ref. [100].

In its current version the CQC Hamiltonian Eq. (2) is formulated in the laboratory frame of reference. The deformation of single-nucleon orbitals is not static, rather it is induced dynamically by the quadrupole and octupole coupling terms in Eq. (5). In the Appendix of Ref. [101] an example for transforming the quadrupole coupling term to the principal-axis system of the core (intrinsic frame) is discussed (cf. Eq. (A2) in Ref. [101]). By combining the resulting deformed potential with the spherical quasiparticle Hamiltonian, one obtains the familiar form of the quasiparticle rotor model. Similarly, in

the model used in the present work the quadrupole-quadrupole and octupole-octupole interactions between the core nucleus and the odd-nucleon in Eq. (5) will play the same role and induce the right deformation for the odd-nucleon orbitals.

The electromagnetic multipole operator consists of single-nucleon and collective parts:

$$
\hat{M}_{\lambda\nu} = \hat{M}_{\lambda\nu}^{\mathrm{s.p.}} + \hat{M}_{\lambda\nu}^{\mathrm{c}}. \tag{8}
$$

The corresponding reduced transition matrix element between states $|\alpha_i J_i \pi_i\rangle$ and $|\alpha_f J_f \pi_f\rangle$ reads

$$
\langle \alpha_f J_f \pi_f \| \hat{M}_\lambda \| \alpha_i J_i \pi_i \rangle = \sqrt{(2J_f + 1)(2J_i + 1)} \sum_{\Omega, \mu_f \mu_i} (-1)^{j_f + J_i + R + \lambda} \begin{Bmatrix} J_f & \lambda & J_i \\ j_i & R & j_f \end{Bmatrix} [M_U^{\mathrm{s.p.}} + M_V^{\mathrm{s.p.}}]
$$
$$
+ \sqrt{(2J_f + 1)(2J_i + 1)} \sum_{\mu, \Omega_f \Omega_i} (-1)^{R_f + J_i + j + \lambda} \begin{Bmatrix} J_f & \lambda & J_i \\ R_i & j & R_f \end{Bmatrix} [M_U^{\mathrm{c}} + M_V^{\mathrm{c}}] \tag{9}
$$

with

$$
M_U^{\mathrm{s.p.}} = U_{\mu_f \Omega}^f U_{\mu_i \Omega}^i \langle \mu_f \| \hat{M}_\lambda^{\mathrm{s.p.}} \| \mu_i \rangle^{A-1}, \tag{10}
$$

$$
M_V^{\mathrm{s.p.}} = V_{\mu_f \Omega}^f V_{\mu_i \Omega}^i \langle \mu_f \| \hat{M}_\lambda^{\mathrm{s.p.}} \| \mu_i \rangle^{A+1}, \tag{11}
$$

$$
M_U^{\mathrm{c}} = U_{\mu \Omega_f}^f U_{\mu \Omega_i}^i \langle \Omega_f \| \hat{M}_\lambda^{\mathrm{c}} \| \Omega_i \rangle^{A-1}, \tag{12}
$$

$$
M_V^{\mathrm{c}} = V_{\mu \Omega_f}^f V_{\mu \Omega_i}^i \langle \Omega_f \| \hat{M}_\lambda^{\mathrm{c}} \| \Omega_i \rangle^{A+1}. \tag{13}
$$

The explicit expressions for the reduced matrix elements of the electric dipole, quadrupole, and octupole operators are given in Sec. II B.

B. Microscopic inputs based on covariant EDFs

The full dynamics of the CQC Hamiltonian Eq. (2) is determined by the energies $\varepsilon_\mu^{A\pm1}$ and $E_\Omega^{A\pm1}$, quadrupole matrix elements $\langle \mu \| \hat{Q}_2 \| \mu' \rangle^{A\pm1}$ and $\langle \Omega \| \hat{Q}_2 \| \Omega' \rangle^{A\pm1}$, octupole matrix elements $\langle \mu \| \hat{Q}_3 \| \mu' \rangle^{A\pm1}$ and $\langle \Omega \| \hat{Q}_3 \| \Omega' \rangle^{A\pm1}$, and pairing gaps $\Delta_\Omega^{A\pm1}$. In the following the superscript $A \pm 1$ will be omitted for convenience. In this particular study we will calculate the input for the CQC model using an axially reflection-asymmetric implementation of the relativistic Hartree-Bogoliubov (RHB) model [29], combined with the quadrupole-octupole collective Hamiltonian [52]. The RHB model provides a unified description of particle-hole (ph) and particle-particle (pp) correlations on a mean-field level by combining two average potentials: the self-consistent mean field that encloses long range ph correlations and a pairing field $\hat{\Delta}$ which sums up pp correlations. In the present

analysis, the mean-field potential is determined by the relativistic density functional PC-PK1 [102] in the ph channel, and a separable pairing force [103] is used in the pp channel. PC-PK1 denotes a parametrization for the covariant nuclear energy density functional with nonlinear point-coupling interactions, that was adjusted in a fit to ground-state properties of 60 selected spherical nuclei, including binding energies, charge radii, and empirical pairing gaps [102].

In the first step of the construction of the CQC Hamiltonian (2), a constrained RHB calculation for spherical configurations of the even-mass cores is carried out to determine the single-nucleon states $|\mu\rangle$ and corresponding energies ε_μ, and the quadrupole ($\lambda = 2$) and octupole ($\lambda = 3$) matrix elements

$$
\langle \mu \| \hat{Q}_\lambda \| \mu' \rangle = \langle n_\mu j \| r^\lambda Y_\lambda \| n_\mu' j' \rangle
$$
$$
= (-1)^{j+j'+\lambda+1} \sqrt{\frac{(2\lambda + 1)(2j' + 1)}{4\pi}}
$$
$$
\times C_{j' \frac{1}{2} \lambda 0}^{j \frac{1}{2}} \langle n_\mu j | r^\lambda | n_\mu' j' \rangle, \tag{14}
$$

where $C_{j' \frac{1}{2} \lambda 0}^{j \frac{1}{2}}$ are the corresponding Clebsch-Gordan coefficients.

In the next step a constrained, axially reflection-asymmetric RHB calculation for the entire energy surface as function of the quadrupole deformation β_2 and octupole deformation β_3 is performed to compute the microscopic input, i.e., the moments of inertia $\mathcal{I}$, collective masses B_{22}, B_{23}, B_{33}, and the potential V_{coll} for the quadrupole-octupole

collective Hamiltonian (QOCH) of the even-mass core [52]:

$$
\hat{H}_{\text{coll}} = -\frac{\hbar^2}{2\sqrt{w\mathcal{I}}}\left[\frac{\partial}{\partial\beta_2}\sqrt{\frac{\mathcal{I}}{w}}B_{33}\frac{\partial}{\partial\beta_2} - \frac{\partial}{\partial\beta_2}\sqrt{\frac{\mathcal{I}}{w}}B_{23}\frac{\partial}{\partial\beta_3} \right.
$$
$$
\left. - \frac{\partial}{\partial\beta_3}\sqrt{\frac{\mathcal{I}}{w}}B_{23}\frac{\partial}{\partial\beta_2} + \frac{\partial}{\partial\beta_3}\sqrt{\frac{\mathcal{I}}{w}}B_{22}\frac{\partial}{\partial\beta_3} \right]
$$
$$
+ \frac{\hat{J}_\perp^2}{2\mathcal{I}} + V_{\text{coll}}(\beta_2,\beta_3). \tag{15}
$$

$\hat{J}_\perp$ denotes the component of angular momentum perpendicular to the symmetric axis in the body-fixed frame of the core. The Coriolis interaction is contained in the rotational term of QOCH because of $J_\perp = J - j$, where J and j are the total angular momentum of the odd-A nucleus and angular momentum of the single nucleon, respectively. In addition to the rotational term, we also include the vibrational term and the collective potential in Eq. (15), and this enables a description of more complex excitation modes, e.g., phonon excitations and shape coexistence. The additional quantity that appears in the vibrational kinetic energy, $w = B_{22}B_{33} - B_{23}^2$, determines the volume element in the collective space,

$$
\int d\tau_{\text{coll}} = \int \sqrt{w\mathcal{I}}\, d\beta_2 d\beta_3 d\Theta, \tag{16}
$$

where Θ are the Euler angles.

The eigenvalue problem of the collective Hamiltonian (15) is solved using an expansion of eigenfunctions in terms of a complete set of basis functions that depend on the collective coordinates β_2, β_3, and Θ [52]. The collective wave functions are thus obtained as

$$
\Psi_\Omega(\beta_2,\beta_3,\Theta) = \psi_{n_\Omega R\pi_R}(\beta_2,\beta_3)|RM_R0\rangle. \tag{17}
$$

The corresponding reduced matrix elements and average pairing gaps are calculated using the expressions

$$
\langle\Omega\|\hat{Q}_\lambda\|\Omega'\rangle = \sqrt{2R+1}\, C_{R'0\lambda0}^{R0}
$$
$$
\times \int d\beta_2 d\beta_3 \sqrt{w\mathcal{I}}\,\psi_{n'_\Omega R'\pi'_R}q_\lambda(\beta_2,\beta_3)\psi^*_{n_\Omega R\pi_R} \tag{18}
$$

$$
\Delta_\Omega = \int d\beta_2 d\beta_3 \sqrt{w\mathcal{I}}\,\big|\psi_{n_\Omega R\pi_R}\big|^2 \Delta(\beta_2,\beta_3), \tag{19}
$$

where $q_\lambda(\beta_2,\beta_3)$ and $\Delta(\beta_2,\beta_3)$ are the mass quadrupole ($\lambda = 2$) and octupole ($\lambda = 3$) moments and pairing gaps, respectively, computed from the RHB intrinsic state at each point on the deformation surface (β_2,β_3).

In the case of electric dipole transitions the reduced matrix elements for the single-nucleon states are calculated from

$$
\langle\mu\|\hat{D}_1\|\mu'\rangle = e_\tau(-1)^{j+j'}\sqrt{\frac{3(2j'+1)}{4\pi}}C_{j'\frac{1}{2}10}^{j\frac{1}{2}}\langle n_\mu j|r|n'_\mu j'\rangle \tag{20}
$$

with $e_\tau = \frac{N}{A}e$ for the odd proton and $e_\tau = -\frac{Z}{A}e$ for the odd neutron. For the even-even core:

$$
\langle\Omega\|\hat{D}_1\|\Omega'\rangle = \sqrt{2R+1}\, C_{R'010}^{R0}
$$
$$
\times \int d\beta_2 d\beta_3 \sqrt{w\mathcal{I}}\,\psi_{n'_\Omega R'\pi_R}D_1(\beta_2,\beta_3)\psi^*_{n_\Omega R\pi_R}, \tag{21}
$$

where $D_1(\beta_2,\beta_3)$ is the electric dipole moment calculated from the RHB intrinsic state using the dipole operator

$$
\hat{D}_1 = \sqrt{\frac{3}{4\pi}}e\left(\frac{N}{A}z_p - \frac{Z}{A}z_n\right). \tag{22}
$$

III. RESULTS AND DISCUSSION

As an illustrative application of the microscopic CQC model, we consider the case of a single neutron coupled to an axially symmetric octupole-deformed even core: the spectroscopy of ^{223,225,227}Ra, for which extensive data are available. Furthermore, we note that ^{225}Ra is the nucleus of choice in the search for a permanent electric dipole moment. The corresponding even-core nuclei $^{222-228}$Ra present good examples of axially symmetric octupole-deformed systems, as shown by the deformation energy surfaces in Fig. 1. All four core nuclei $^{222-228}$Ra exhibit a global minimum with $\beta_3 > 0.1$ and octupole deformation energy $\Delta E_{\text{oct}} > 0.4$ MeV. As the neutron number increases, both the octupole deformation and ΔE_{oct} increase from ^{222}Ra to ^{226}Ra, and then start to decrease from ^{228}Ra. The isotope ^{226}Ra exhibits the deepest octupole minimum with $\Delta E_{\text{oct}} \approx 0.94$ MeV. Similar deformation energy surfaces of Ra isotopes have also been obtained
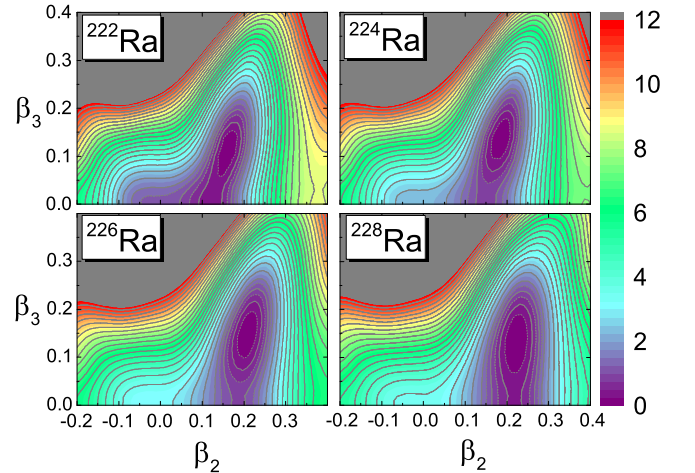
FIG. 1. Self-consistent RHB deformation energy surfaces of the core nuclei $^{222-228}$Ra in the β_2-β_3 plane. For each nucleus the energies are normalized with respect to the binding energy of the global minimum. The contours join points on the surface with the same energy (in MeV). Contour lines are separated by 0.5 MeV (between neighboring solid lines) and 0.25 MeV (between neighboring dashed and solid lines), respectively.
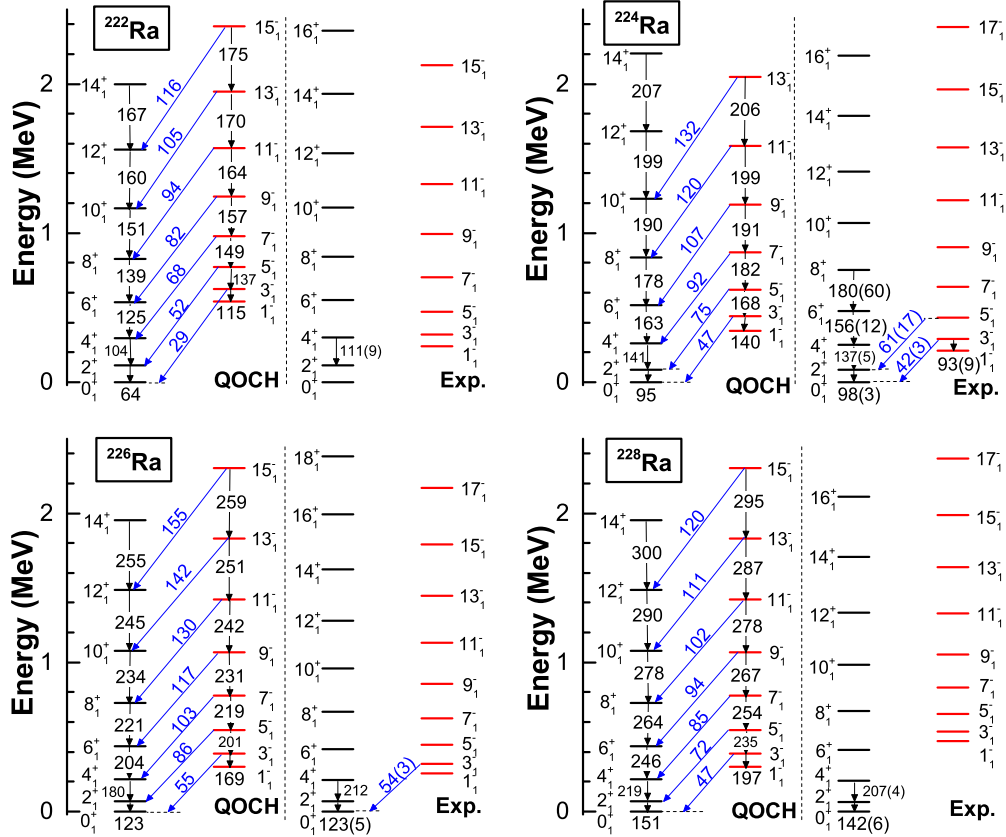
FIG. 2. The excitation spectrum, intraband $B(E2)$ values (in W.u.), and interband $B(E3)$ values (in W.u.) of the core nuclei $^{222-228}$Ra calculated with the QOCH based on the PC-PK1 relativistic density functional and compared to experimental results [1,104].

in the RHB calculation with the DD-PC1 functional,[1] but in that case the most pronounced octupole minimum has been obtained for ^{224}Ra [45].

The solution of the eigenvalue equations for the corresponding quadrupole-octupole collective Hamiltonian yields the collective excitation spectra of the even-core nuclei. Figure 2 displays the resulting excitation energies, intraband $B(E2)$ values, and interband $B(E3)$ values for the ground-state bands and lowest-lying negative-parity bands. Except for the calculated negative-parity band heads in ^{222}Ra and ^{228}Ra being somewhat higher and lower than the corresponding experimental counterparts, respectively, the overall structure agrees very well with the available data. It should be emphasized that the electric transition rates are in excellent agreement with data. This is relevant for the calculation of odd-A nuclei using the CQC model, because it includes the reduced quadrupole and octupole matrix elements as input.

The next step is the construction of the CQC Hamiltonian. The fermion space consists of spherical single-neutron states with $E_f^{\mathrm{sph}} - 2\hbar\omega \leqslant \varepsilon_\mu \leqslant 2$ MeV, where E_f^{sph} is the

Fermi surface of the corresponding spherical configuration and $\hbar\omega = 41A^{-\frac{1}{3}}$ MeV. Both positive- and negative-parity single-neutron states in the canonical basis are included. For

FIG. 3. Quasiparticle energies [eigenenergies of H_{qp} in Eq. (2)] relevant for the bandheads of the low-energy spectra of ^{223}Ra: $J^\pi = 1/2^\pm$, $3/2^\pm$, and $5/2^\pm$, as functions of the octupole coupling strength χ_3 ($\chi_2 = 5.5$ MeV/b^2).

---

[1]DD-PC1 denotes a parametrization for the covariant nuclear energy density functional with density-dependent point-coupling interactions. It was adjusted in a fit to the experimental masses of a set of 64 deformed nuclei in the mass regions $A \approx 150$–180 and $A \approx 230$–250 [105].
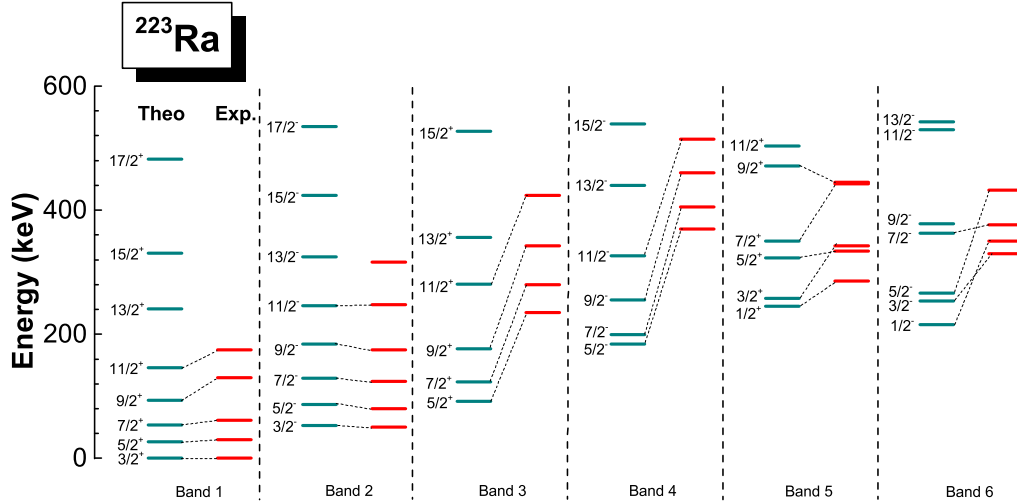
FIG. 4. The low-lying excitation spectrum of the odd-mass nucleus ^{223}Ra calculated with the CQC model, plotted in comparison with available experimental data [104]. The following values of the Fermi surface and coupling strengths are adjusted to low-energy data: $\varepsilon_f = -6.36$ MeV, $\chi_2 = 5.5$ MeV/b^2, $\chi_3 = 4.0$ MeV/b^3.

TABLE I. The probabilities of the dominant configurations in the wave functions of selected states in the ground-state band and band 2 of ^{223}Ra.

J^π	$j \otimes R$	$A-1$	$A+1$	J^π	$j \otimes R$	$A-1$	$A+1$
$3/2^+$	$3d_{5/2} \otimes 2_1^+$	0.07	0.10	$3/2^-$	$3d_{5/2} \otimes 1_1^-$	0.02	0.07
	$2g_{9/2} \otimes 4_1^+$	0.23	0.27		$3d_{5/2} \otimes 3_1^-$	0.03	0.07
					$2g_{9/2} \otimes 3_1^-$	0.07	0.15
					$2g_{9/2} \otimes 5_1^-$	0.10	0.22
					$1i_{11/2} \otimes 5_1^-$	0.04	0.09
$5/2^+$	$2g_{9/2} \otimes 2_1^+$	0.12	0.11	$5/2^-$	$3d_{5/2} \otimes 3_1^-$	0.02	0.09
	$1i_{11/2} \otimes 4_1^+$	0.08	0.16		$2g_{9/2} \otimes 3_1^-$	0.09	0.12
	$2g_{9/2} \otimes 6_1^+$	0.11	0.14		$1i_{11/2} \otimes 3_1^-$	0.02	0.09
					$2g_{9/2} \otimes 5_1^-$	0.04	0.16
					$2g_{9/2} \otimes 7_1^-$	0.02	0.06
$7/2^+$	$1i_{11/2} \otimes 2_1^+$	0.12	0.23	$7/2^-$	$3d_{5/2} \otimes 1_1^-$	0.01	0.05
	$2g_{9/2} \otimes 4_1^+$	0.05	0.04		$2g_{9/2} \otimes 1_1^-$	0.06	0.08
	$1i_{11/2} \otimes 4_1^+$	0.08	0.02		$1i_{11/2} \otimes 3_1^-$	0.09	0.15
	$2g_{9/2} \otimes 6_1^+$	0.01	0.07		$3d_{5/2} \otimes 5_1^-$	0.03	0.05
	$1i_{11/2} \otimes 6_1^+$	0.01	0.11		$1i_{11/2} \otimes 5_1^-$	0.00	0.06
					$2g_{9/2} \otimes 7_1^-$	0.04	0.17
$9/2^+$	$1i_{11/2} \otimes 2_1^+$	0.21	0.17	$9/2^-$	$1i_{11/2} \otimes 1_1^-$	0.11	0.20
	$1i_{11/2} \otimes 4_1^+$	0.03	0.17		$2g_{9/2} \otimes 5_1^-$	0.04	0.06
	$2g_{9/2} \otimes 8_1^+$	0.02	0.06		$1i_{11/2} \otimes 5_1^-$	0.06	0.05
	$1i_{11/2} \otimes 8_1^+$	0.00	0.05		$2g_{9/2} \otimes 7_1^-$	0.00	0.07
					$1i_{11/2} \otimes 7_1^-$	0.00	0.07
$11/2^+$	$1i_{11/2} \otimes 0_1^+$	0.19	0.20	$11/2^-$	$1i_{11/2} \otimes 1_1^-$	0.09	0.06
	$1i_{11/2} \otimes 2_1^+$	0.01	0.09		$1i_{11/2} \otimes 3_1^-$	0.11	0.16
	$1i_{11/2} \otimes 4_1^+$	0.08	0.00		$1i_{11/2} \otimes 5_1^-$	0.00	0.10
	$1i_{11/2} \otimes 6_1^+$	0.04	0.08		$2g_{9/2} \otimes 9_1^-$	0.01	0.09
	$1i_{11/2} \otimes 8_1^+$	0.01	0.07				
$13/2^+$	$1i_{11/2} \otimes 2_1^+$	0.19	0.11	$13/2^-$	$1i_{11/2} \otimes 1_1^-$	0.16	0.22
	$1i_{11/2} \otimes 4_1^+$	0.08	0.17		$1i_{11/2} \otimes 5_1^-$	0.10	0.01
	$1i_{11/2} \otimes 6_1^+$	0.01	0.08		$1i_{11/2} \otimes 7_1^-$	0.01	0.08
	$1i_{11/2} \otimes 10_1^+$	0.01	0.06				

the collective states of the core nuclei, we include the following states: $0_1^+, 2_1^+, \ldots, 18_1^+$ in the positive-parity ground-state band and $1_1^-, 3_1^-, \ldots, 17_1^-$ in the lowest negative-parity band.

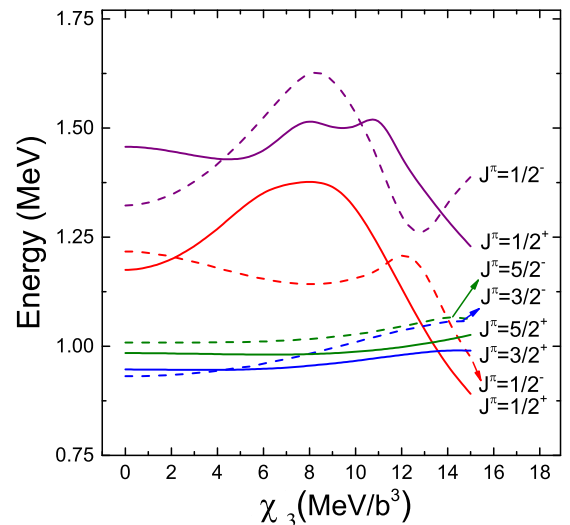Before discussing the full spectrum, in Fig. 3 we show the evolution of quasiparticle energies [eigenenergies of H_{qp} in Eq. (2)] relevant for the bandheads of the low-energy spectra of ^{223}Ra: $J^\pi = 1/2^\pm$, $3/2^\pm$, and $5/2^\pm$, as functions of the octupole coupling strength χ_3. One clearly observes the parity doublet structure of the bandheads. In particular, we note the pronounced dependence of the $J^\pi = 1/2^\pm$ states on the strength of the octupole interaction.

On this and the following pages we group, by isotope, the figures with the excitation spectra and the tables with the dominant configurations. Figure 4 displays the low-lying excitation spectrum of the odd-mass nucleus ^{223}Ra calculated with the CQC model, in comparison with available experimental data [104]. The levels are grouped into different bands according to the dominant decay pattern. Here six low-lying bands with bandheads $J^\pi = 3/2^\pm$, $J^\pi = 5/2^\pm$, and $J^\pi = 1/2^\pm$ are shown, and they are displayed as three parity doublets. The ground-state band and its partner are well reproduced by the CQC model, especially the very small energy difference ≈ 50 keV between the two bandheads. In Table I we also list the probabilities of dominant configurations in the wave functions of selected states in the ground-state band and band 2 of ^{223}Ra. The parity doublet is dominated by the strongly mixed configurations of $3d_{5/2}$ and $2g_{9/2}$ for the low-spin states, and gradually the $1i_{11/2}$ configuration becomes dominant for high-spin states. Note that both the ground-state band and band 2 are predominantly built by coupling the single neutron to the corresponding positive-parity and negative-parity bands in the core nuclei, respectively. There is no mixing between opposite-parity bands of the cores in the yrast states, and this points to weaker octupole correlations compared to ^{225}Ra and ^{227}Ra below. For the second parity doublet, i.e., bands 3 and 4, in Fig. 4 the overall structure is reproduced but the theoretical bandheads are ≈ 130 keV lower than the corresponding experimental levels. We can also obtain the $J^\pi = 1/2^\pm$
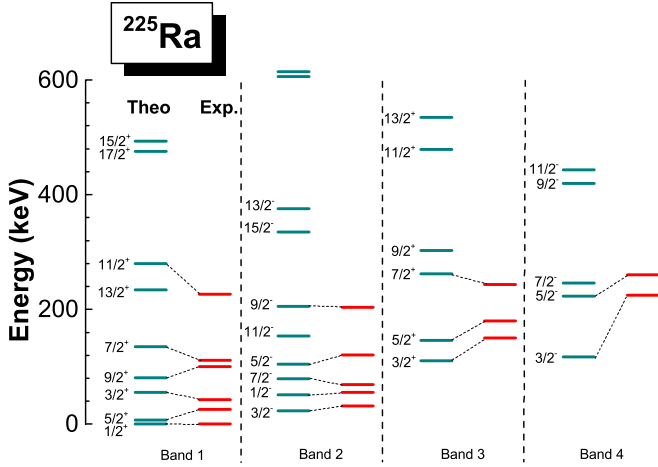
FIG. 5. The same as in Fig. 4 but for ^{225}Ra. The Fermi surface and coupling strengths read $\varepsilon_f = -4.56$ MeV, $\chi_2 = 6.9$ MeV/b^2, $\chi_3 = 22.8$ MeV/b^3.

parity doublet and compare it with the experimental spectrum. However, the theoretical results exhibit opposite staggering, possibly due to a weaker Coriolis coupling, and this could be solved by adding a magnetic dipole particle-core interaction term [106].

In Fig. 5 and Table II we display the excitation spectrum and the dominant configurations in the wave functions of

TABLE II. The same as in Table I but for ^{225}Ra.

J^π	$j \otimes R$	$A-1$	$A+1$	J^π	$j \otimes R$	$A-1$	$A+1$
$1/2^+$	$3d_{5/2} \otimes 2_1^+$	0.18	0.12	$1/2^-$	$3d_{5/2} \otimes 3_1^-$	0.18	0.11
	$1i_{11/2} \otimes 6_1^+$	0.11	0.06		$2g_{7/2} \otimes 3_1^-$	0.06	0.02
	$1j_{15/2} \otimes 7_1^-$	0.14	0.08		$1i_{11/2} \otimes 5_1^-$	0.10	0.06
					$1j_{15/2} \otimes 8_1^+$	0.14	0.09
$3/2^+$	$3d_{5/2} \otimes 2_1^+$	0.09	0.08	$3/2^-$	$3d_{5/2} \otimes 1_1^-$	0.14	0.10
	$2g_{7/2} \otimes 4_1^+$	0.07	0.05		$1j_{15/2} \otimes 6_1^+$	0.15	0.13
	$1i_{11/2} \otimes 6_1^+$	0.07	0.05		$1i_{11/2} \otimes 7_1^-$	0.09	0.05
	$1j_{15/2} \otimes 7_1^-$	0.14	0.15				
$5/2^+$	$3d_{5/2} \otimes 0_1^+$	0.09	0.06	$5/2^-$	$3d_{5/2} \otimes 3_1^-$	0.07	0.06
	$3d_{5/2} \otimes 2_1^+$	0.06	0.04		$2g_{7/2} \otimes 5_1^-$	0.06	0.06
	$1j_{15/2} \otimes 5_1^-$	0.14	0.11		$1j_{15/2} \otimes 6_1^+$	0.10	0.11
	$1i_{11/2} \otimes 8_1^+$	0.10	0.05		$1i_{11/2} \otimes 7_1^-$	0.05	0.04
					$1j_{15/2} \otimes 8_1^+$	0.07	0.07
$7/2^+$	$3d_{5/2} \otimes 4_1^+$	0.06	0.05	$7/2^-$	$3d_{5/2} \otimes 1_1^-$	0.11	0.07
	$1j_{15/2} \otimes 5_1^-$	0.08	0.07		$1j_{15/2} \otimes 4_1^+$	0.14	0.12
	$2g_{7/2} \otimes 6_1^+$	0.05	0.05		$1i_{11/2} \otimes 9_1^-$	0.09	0.04
	$1j_{15/2} \otimes 7_1^-$	0.05	0.07				
$9/2^+$	$3d_{5/2} \otimes 2_1^+$	0.13	0.07	$9/2^-$	$1j_{15/2} \otimes 4_1^+$	0.19	0.08
	$1j_{15/2} \otimes 3_1^-$	0.12	0.10		$1i_{11/2} \otimes 7_1^-$	0.14	0.02
	$1i_{11/2} \otimes 10_1^+$	0.09	0.04				
$11/2^+$	$3d_{5/2} \otimes 4_1^+$	0.06	0.04	$11/2^-$	$1j_{15/2} \otimes 2_1^+$	0.13	0.10
	$1j_{15/2} \otimes 5_1^-$	0.05	0.05		$3d_{5/2} \otimes 3_1^-$	0.13	0.06
					$1i_{11/2} \otimes 11_1^-$	0.08	0.03
$13/2^+$	$1j_{15/2} \otimes 1_1^-$	0.09	0.07	$13/2^-$	$1j_{15/2} \otimes 2_1^+$	0.11	0.03
	$1j_{15/2} \otimes 3_1^-$	0.05	0.05		$1j_{15/2} \otimes 4_1^+$	0.07	0.05
	$3d_{5/2} \otimes 4_1^+$	0.14	0.06		$1i_{11/2} \otimes 9_1^-$	0.12	0.01
	$1i_{11/2} \otimes 12_1^+$	0.09	0.03				

states in ^{225}Ra, respectively. In general, the low-lying excitations and parity doublet structure are reproduced by the CQC model, except the staggering behavior of the ground-state $K = 1/2$ band. The ground state $J^\pi = 1/2^+$ and its parity partner $J^\pi = 1/2^-$ in band 2 are particularly interesting because they are associated with the enhancement of the Schiff moment [23,25]. Here we obtain a good description for both the excitation energy and electric transition rates, as shown in Table IV. In Table II the pronounced mixing between positive- and negative-parity single-particle states and collective states of the cores reflects a strong octupole coupling between the odd neutron and the even-even cores.

Figure 6 and Table III contain the results for ^{227}Ra. The structure of bands is similar to that found in ^{223,225}Ra. Bands 1, 2 and bands 3, 4 form two parity-doublet sequences. The low-lying band 5 is also reproduced but the partner band of opposite parity has not been determined in experiment. Band 6 is the corresponding theoretical prediction. The ground-state band and its partner band in ^{227}Ra are characterized by pronounced octupole correlations that are reflected in the mixing of positive- and negative-parity core states. One also notices that the lowest band structure of ^{227}Ra is mainly built on the configurations with a neutron hole coupled to the heavier core ^{228}Ra.

Tables IV and V collect the results for intraband and interband electric quadrupole $E2$ transition rates and interband electric dipole $E1$ and octupole $E3$ transition rates for ^{223,225,227}Ra. The overall agreement between theoretical predictions and experiment values is satisfactory, especially considering that the present calculation includes the full configuration space and, therefore, does not contain adjustable parameters in the form of effective charges. More specifically, most of the intraband $E2$ transition rates are reproduced very well, while the calculated interband $B(E2)$ values appear to be somewhat smaller than the experimental values. The theoretical $B(E1)$ values are generally large when compared to the data, but they are of the same order of magnitude. Some of these values are large, which is consistent with the pronounced octupole correlations predicted in these nuclei. Octupole correlations can be quantified by the calculated $E3$ transition rates in Table V, where rather large $B(E3)$ values are predicted and they increase with angular momentum. In the Supplemental Material [107] we also include model predictions for the intraband and interband $B(E2)$, and interband $B(E1)$, and $B(E3)$ values of ^{223,225,227}Ra in Tables S1, S2, and S3, respectively.

IV. SUMMARY

In summary, we have extended our microscopic CQC model to odd-mass nuclei characterized by both quadrupole and octupole shape deformations. The dynamics of the CQC Hamiltonian is determined by microscopically calculated single-nucleon and collective energies, quadrupole and octupole matrix elements, and pairing gaps corresponding to collective states of the even-mass core nuclei and spherical single-particle states of the odd nucleon. These are calculated using a quadrupole-octupole collective core Hamiltonian combined with a constrained relativistic Hartree-Bogoliubov
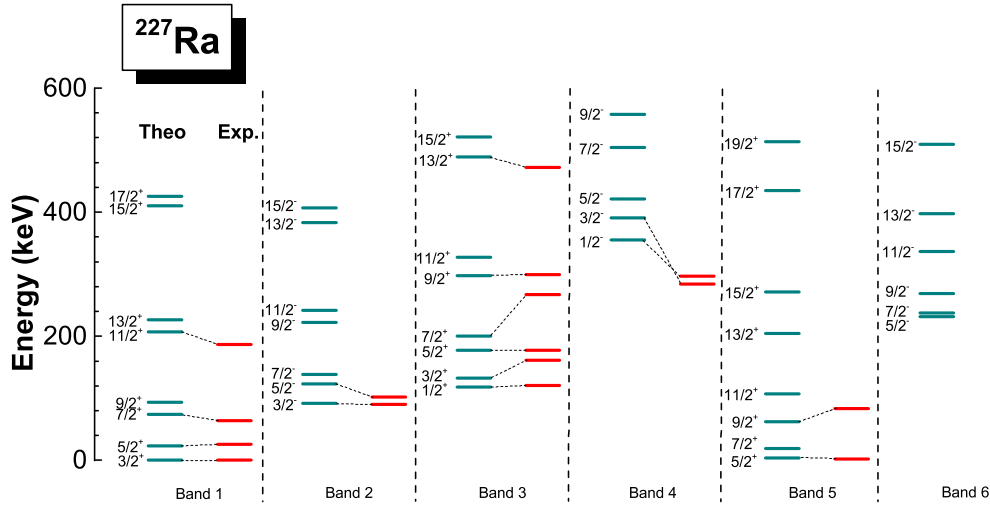
FIG. 6. The same as in Fig. 4 but for ^{227}Ra. The Fermi surface and coupling strengths read $\varepsilon_f = -6.28$ MeV, $\chi_2 = 4.8$ MeV/b^2, $\chi_3 = 12.5$ MeV/b^3.

model. The relativistic density functional PC-PK1 has been employed in the particle-hole channel, and a separable pairing force in the particle-particle channel. In the present version

TABLE III. The same as in Table I but for ^{227}Ra.

J^π	$j \otimes R$	$A-1$	$A+1$	J^π	$j \otimes R$	$A-1$	$A+1$
$3/2^+$	$3p_{3/2} \otimes 1_1^-$	0.02	0.11	$3/2^-$	$3p_{3/2} \otimes 0_1^+$	0.02	0.20
	$3d_{5/2} \otimes 2_1^+$	0.03	0.13		$3d_{5/2} \otimes 1_1^-$	0.00	0.13
	$2g_{9/2} \otimes 4_1^+$	0.05	0.17		$2g_{9/2} \otimes 3_1^-$	0.03	0.08
	$1i_{11/2} \otimes 4_1^+$	0.01	0.06				
	$1i_{11/2} \otimes 6_1^+$	0.03	0.09				
	$1j_{15/2} \otimes 7_1^-$	0.01	0.09				
$5/2^+$	$3d_{5/2} \otimes 0_1^+$	0.01	0.07	$5/2^-$	$3p_{3/2} \otimes 2_1^+$	0.02	0.22
	$3p_{3/2} \otimes 1_1^-$	0.01	0.06		$3d_{5/2} \otimes 3_1^-$	0.01	0.11
	$2g_{9/2} \otimes 2_1^+$	0.05	0.13		$2g_{9/2} \otimes 3_1^-$	0.05	0.07
	$1j_{15/2} \otimes 5_1^-$	0.02	0.07		$2g_{9/2} \otimes 5_1^-$	0.00	0.05
	$1i_{11/2} \otimes 6_1^+$	0.02	0.17				
$7/2^+$	$3d_{5/2} \otimes 2_1^+$	0.02	0.06	$7/2^-$	$3d_{5/2} \otimes 1_1^-$	0.00	0.12
	$2g_{9/2} \otimes 2_1^+$	0.07	0.07		$2g_{9/2} \otimes 1_1^-$	0.05	0.09
	$3p_{3/2} \otimes 3_1^-$	0.01	0.09		$3p_{3/2} \otimes 2_1^+$	0.01	0.18
	$3d_{5/2} \otimes 4_1^+$	0.00	0.05				
	$2g_{9/2} \otimes 4_1^+$	0.02	0.08				
	$1j_{15/2} \otimes 5_1^-$	0.04	0.06				
	$1i_{11/2} \otimes 8_1^+$	0.01	0.10				
$9/2^+$	$2g_{9/2} \otimes 0_1^+$	0.06	0.10	$9/2^-$	$3d_{5/2} \otimes 3_1^-$	0.01	0.08
	$3d_{5/2} \otimes 2_1^+$	0.01	0.12		$3p_{3/2} \otimes 4_1^+$	0.02	0.19
	$2g_{9/2} \otimes 2_1^+$	0.02	0.06		$3d_{5/2} \otimes 5_1^-$	0.00	0.07
	$3p_{3/2} \otimes 3_1^-$	0.01	0.08		$2g_{9/2} \otimes 5_1^-$	0.01	0.05
	$1j_{15/2} \otimes 3_1^-$	0.05	0.07				
$11/2^+$	$2g_{9/2} \otimes 2_1^+$	0.06	0.04	$11/2^-$	$2g_{9/2} \otimes 1_1^-$	0.05	0.08
	$3d_{5/2} \otimes 4_1^+$	0.01	0.07		$1j_{15/2} \otimes 2_1^+$	0.06	0.03
	$2g_{9/2} \otimes 4_1^+$	0.05	0.07		$3d_{5/2} \otimes 3_1^-$	0.00	0.15
	$3p_{3/2} \otimes 5_1^-$	0.01	0.08		$3p_{3/2} \otimes 4_1^+$	0.01	0.17
	$1i_{11/2} \otimes 10_1^+$	0.00	0.08				
$13/2^+$	$1j_{15/2} \otimes 1_1^-$	0.05	0.05	$13/2^-$	$1i_{11/2} \otimes 1_1^-$	0.07	0.10
	$2g_{9/2} \otimes 2_1^+$	0.08	0.14		$3d_{5/2} \otimes 5_1^-$	0.01	0.05
	$3d_{5/2} \otimes 4_1^+$	0.00	0.14		$3p_{3/2} \otimes 6_1^+$	0.01	0.13
	$3p_{3/2} \otimes 5_1^-$	0.01	0.09		$3d_{5/2} \otimes 7_1^-$	0.00	0.05

of the model the free parameters—the Fermi energy ε_f and particle-vibration coupling strengths χ_2 and χ_3—are specifically adjusted to the experimental excitation energies of few lowest states. The model has been put to the test in a study of low-lying excitation spectra for the odd-A nuclei $^{223-227}$Ra. The theoretical results reproduce the available data on band structure, especially the parity doublets, intraband

TABLE IV. Theoretical intraband and interband $E2$ and interband $E1$ transition rates (in Weisskopf units) for low-lying bands in ^{223,225,227}Ra, in comparison with available experimental values [104].

		Theory	Experiment
^{223}Ra	$B(E1; 3/2^-_{\text{band2}} \to 5/2^+_{\text{band1}})$	0.00057	0.00050(9)
	$B(E1; 7/2^-_{\text{band2}} \to 5/2^+_{\text{band1}})$	0.00057	$7.9 \times 10^{-5}(24)$
	$B(E1; 3/2^-_{\text{band6}} \to 1/2^+_{\text{band5}})$	0.00082	0.000160(20)
	$B(E1; 3/2^-_{\text{band6}} \to 5/2^+_{\text{band5}})$	0	$5.2 \times 10^{-6}(6)$
	$B(E2; 7/2^+_{\text{band1}} \to 5/2^+_{\text{band1}})$	86.59	70
	$B(E2; 11/2^+_{\text{band1}} \to 7/2^+_{\text{band1}})$	74.80	$2.8 \times 10^2(12)$
	$B(E2; 7/2^+_{\text{band1}} \to 3/2^+_{\text{band1}})$	31.48	44
	$B(E2; 7/2^-_{\text{band2}} \to 5/2^-_{\text{band2}})$	107.90	$1.1 \times 10^2(5)$
	$B(E2; 7/2^-_{\text{band2}} \to 3/2^-_{\text{band2}})$	60.56	10(6)
	$B(E2; 3/2^-_{\text{band6}} \to 5/2^-_{\text{band2}})$	0.042	0.91(15)
	$B(E2; 3/2^-_{\text{band6}} \to 7/2^-_{\text{band2}})$	0.38	1.65(24)
^{225}Ra	$B(E1; 3/2^-_{\text{band2}} \to 1/2^+_{\text{band1}})$	0.0024	0.00081(20)
	$B(E2; 3/2^+_{\text{band1}} \to 1/2^+_{\text{band1}})$	55.89	>2.0
	$B(E2; 5/2^+_{\text{band1}} \to 1/2^+_{\text{band1}})$	91.54	102(6)
^{227}Ra	$B(E1; 3/2^-_{\text{band2}} \to 5/2^+_{\text{band1}})$	0.0037	0.00060(9)
	$B(E1; 5/2^-_{\text{band2}} \to 7/2^+_{\text{band1}})$	0.0058	0.0010(3)
	$B(E1; 5/2^-_{\text{band2}} \to 3/2^+_{\text{band1}})$	0.0084	0.00030(7)
	$B(E1; 3/2^-_{\text{band4}} \to 5/2^+_{\text{band3}})$	0.0012	>0.00067
	$B(E1; 3/2^-_{\text{band4}} \to 1/2^+_{\text{band3}})$	0.00093	>0.00050
	$B(E1; 1/2^-_{\text{band4}} \to 3/2^+_{\text{band3}})$	0.0023	>0.00045
	$B(E1; 1/2^-_{\text{band4}} \to 3/2^+_{\text{band1}})$	8.3×10^{-7}	$>1.3 \times 10^{-6}$
	$B(E2; 3/2^-_{\text{band4}} \to 5/2^-_{\text{band2}})$	0.14	>4.3

TABLE V. Calculated $E3$ transition rates (in Weisskopf units) for low-lying energy levels from band 2 to the ground-state band in ^{223,225,227}Ra.

		Th.		Th.
^{223}Ra	$B(E3; 9/2_1^- \to 3/2_1^+)$	16.76	$B(E3; 11/2_1^- \to 5/2_1^+)$	27.88
	$B(E3; 13/2_1^- \to 7/2_1^+)$	37.38	$B(E3; 15/2_1^- \to 9/2_1^+)$	47.56
	$B(E3; 17/2_1^- \to 11/2_1^+)$	53.81	$B(E3; 19/2_1^- \to 13/2_1^+)$	63.64
	$B(E3; 21/2_1^- \to 15/2_1^+)$	64.20		
^{225}Ra	$B(E3; 7/2_1^- \to 1/2_1^+)$	38.26	$B(E3; 9/2_1^- \to 3/2_1^+)$	29.27
	$B(E3; 11/2_1^- \to 5/2_1^+)$	71.21	$B(E3; 13/2_1^- \to 7/2_1^+)$	60.78
	$B(E3; 15/2_1^- \to 9/2_1^+)$	83.75	$B(E3; 17/2_1^- \to 11/2_1^+)$	79.58
	$B(E3; 19/2_1^- \to 13/2_1^+)$	90.93	$B(E3; 21/2_1^- \to 15/2_1^+)$	97.79
^{227}Ra	$B(E3; 9/2_1^- \to 3/2_1^+)$	26.11	$B(E3; 11/2_1^- \to 5/2_2^+)$	30.84
	$B(E3; 13/2_1^- \to 7/2_2^+)$	36.75	$B(E3; 15/2_1^- \to 9/2_2^+)$	65.15
	$B(E3; 17/2_1^- \to 11/2_2^+)$	66.67	$B(E3; 19/2_1^- \to 13/2_2^+)$	82.99
	$B(E3; 21/2_2^- \to 15/2_2^+)$	81.46		

and interband $B(E2)$, and interband $B(E1)$. The near degeneracy of the parity doublets, pronounced $E1$ transitions, and large predicted $B(E3)$ values indicate the importance of pronounced octupole correlations in the low-energy structure of ^{223,225,227}Ra.

[1] L. P. Gaffney, P. A. Butler, M. Scheck, A. B. Hayes, F. Wenander, M. Albers, B. Bastin, C. Bauer, A. Blazhev, S. Bönig, N. Bree, J. Cederkäll, T. Chupp, D. Cline, T. E. Cocolios, T. Davinson, H. De Witte, J. Diriken, T. Grahn, A. Herzan, M. Huyse, D. G. Jenkins, D. T. Joss, N. Kesteloot, J. Konki, M. Kowalczyk, T. Kröll, E. Kwan, R. Lutter, K. Moschner, P. Napiorkowski, J. Pakarinen, M. Pfeiffer, D. Radeck, P. Reiter, K. Reynders, S. V. Rigby, L. M. Robledo, M. Rudigier, S. Sambi, M. Seidlitz, B. Siebeck, T. Stora, P. Thoele, P. Van Duppen, M. J. Vermeulen, M. von Schmid, D. Voulot, N. Warr, K. Wimmer, K. Wrzosek-Lipska, C. Y. Wu, and M. Zielinska, Studies of pear-shaped nuclei using accelerated radioactive beams, Nature (London) **497**, 199 (2013).

[2] B. Bucher, S. Zhu, C. Y. Wu, R. V. F. Janssens, D. Cline, A. B. Hayes, M. Albers, A. D. Ayangeakaa, P. A. Butler, C. M. Campbell, M. P. Carpenter, C. J. Chiara, J. A. Clark, H. L. Crawford, M. Cromaz, H. M. David, C. Dickerson, E. T. Gregor, J. Harker, C. R. Hoffman, B. P. Kay, F. G. Kondev, A. Korichi, T. Lauritsen, A. O. Macchiavelli, R. C. Pardo, A. Richard, M. A. Riley, G. Savard, M. Scheck, D. Seweryniak, M. K. Smith, R. Vondrasek, and A. Wiens, Direct Evidence of Octupole Deformation in Neutron-Rich ^{144}Ba, Phys. Rev. Lett. **116**, 112503 (2016).

[3] B. Bucher, S. Zhu, C. Y. Wu, R. V. F. Janssens, R. N. Bernard, L. M. Robledo, T. R. Rodríguez, D. Cline, A. B. Hayes, A. D. Ayangeakaa, M. Q. Buckner, C. M. Campbell, M. P. Carpenter, J. A. Clark, H. L. Crawford, H. M. David, C. Dickerson, J. Harker, C. R. Hoffman, B. P. Kay, F. G. Kondev, T. Lauritsen, A. O. Macchiavelli, R. C. Pardo, G. Savard, D. Seweryniak, and R. Vondrasek, Direct Evidence for Octupole Deformation in ^{146}Ba and the Origin of Large $E1$ Moment Variations in Reflection-Asymmetric Nuclei, Phys. Rev. Lett. **118**, 152504 (2017).

[4] P. A. Butler and W. Nazarewicz, Intrinsic reflection asymmetry in atomic nuclei, Rev. Mod. Phys. **68**, 349 (1996).

[5] P. A. Butler, Octupole collectivity in nuclei, J. Phys. G **43**, 073002 (2016).

[6] J. Engel, M. J. Ramsey-Musolf, and U. van Kolck, Electric dipole moments of nucleons, nuclei, and atoms: The standard model and beyond, in *Fundamental Symmetries in the Era of the LHC*, special issue of Prog. Part. Nucl. Phys. **71**, 21 (2013).

[7] T. E. Chupp, P. Fierlinger, M. J. Ramsey-Musolf, and J. T. Singh, Electric dipole moments of atoms, molecules, nuclei, and particles, Rev. Mod. Phys. **91**, 015001 (2019).

[8] J. Dobaczewski, J. Engel, M. Kortelainen, and P. Becker, Correlating Schiff Moments in the Light Actinides with Octupole Moments, Phys. Rev. Lett. **121**, 232501 (2018).

[9] R. Lică, G. Benzoni, A. I. Morales, M. J. G. Borge, L. M. Fraile, H. Mach, M. Madurga, C. Sotty, V. Vedia, H. D. Witte, J. Benito, T. Berry, N. Blasi, A. Bracco, F. Camera, S. Ceruti, V. Charviakova, N. Cieplicka-Oryńczak, C. Costache, F. C. L. Crespi, J. Creswell, G. Fernández-Martínez, H. Fynbo, P. Greenlees, I. Homm, M. Huyse, J. Jolie, V. Karayonchev, U. Köster, J. Konki, T. Kröll, J. Kurcewicz, T. Kurtukian-Nieto, I. Lazarus, S. Leoni, M. Lund, N. Marginean, R. Marginean, C. Mihai, R. Mihai, A. Negret, A. Orduz, Z. Patyk, S. Pascu, V. Pucknell, P. Rahkila, J. M. Regis, F. Rotaru, N. Saed-Sami, V. Sánchez-Tembleque, M. Stanoiu, O. Tengblad, M. Thuerauf, A. Turturica, P. V. Duppen, and N. Warr, β decay studies of

N-rich Cs isotopes with the ISOLDE decay station, J. Phys. G: Nucl. Part. Phys. **44**, 054002 (2017).

[10] J. Wiśniewski, W. Urban, T. Rząca-Urban, A. G. Smith, J. F. Smith, G. S. Simpson, I. Ahmad, and J. P. Greene, Parity-doublet structure in the $^{147}_{57}$La$_{90}$ nucleus, Phys. Rev. C **96**, 064301 (2017).

[11] E. H. Wang, W. Lewis, C. J. Zachary, J. H. Hamilton, A. V. Ramayya, J. K. Hwang, S. H. Liu, N. T. Brewer, Y. X. Luo, J. O. Rasmussen, S. J. Zhu, G. M. Ter-Akopian, and Y. T. Oganessian, New levels and reinvestigation of octupole correlations in ^{146,147}La, Eur. Phys. J. A **53**, 234 (2017).

[12] E. Ruchowska, H. Mach, M. Kowal, J. Skalski, W. A. Płóciennik, and B. Fogelberg, Search for octupole correlations in ^{147}Nd, Phys. Rev. C **92**, 034328 (2015).

[13] H. J. Li, S. J. Zhu, J. H. Hamilton, E. H. Wang, A. V. Ramayya, Y. J. Chen, J. K. Hwang, J. Ranger, S. H. Liu, Z. G. Xiao, Y. Huang, Z. Zhang, Y. X. Luo, J. O. Rasmussen, I. Y. Lee, G. M. Ter-Akopian, Y. T. Oganessian, and W. C. Ma, Reinvestigation of high spin states and proposed octupole correlations in ^{147}Ce, Phys. Rev. C **90**, 047303 (2014).

[14] T. Rząca-Urban, W. Urban, A. G. Smith, I. Ahmad, and A. Syntfeld-Każuch, Unexpected 5/2$^-$ spin of the ground state in ^{147}Ba: No octupole deformation in ground states of odd-*A* Ba isotopes, Phys. Rev. C **87**, 031305(R) (2013).

[15] T. Rzaca-Urban, W. Urban, J. A. Pinston, G. S. Simpson, A. G. Smith, and I. Ahmad, Reflection symmetry of the near-yrast excitations in ^{145}Ba, Phys. Rev. C **86**, 044324 (2012).

[16] X. C. Chen, J. Zhao, C. Xu, H. Hua, T. M. Shneidman, S. G. Zhou, X. G. Wu, X. Q. Li, S. Q. Zhang, Z. H. Li, W. Y. Liang, J. Meng, F. R. Xu, B. Qi, Y. L. Ye, D. X. Jiang, Y. Y. Cheng, C. He, J. J. Sun, R. Han, C. Y. Niu, C. G. Li, P. J. Li, C. G. Wang, H. Y. Wu, Z. H. Li, H. Zhou, S. P. Hu, H. Q. Zhang, G. S. Li, C. Y. He, Y. Zheng, C. B. Li, H. W. Li, Y. H. Wu, P. W. Luo, and J. Zhong, Evolution of octupole correlations in ^{123}Ba, Phys. Rev. C **94**, 021301(R) (2016).

[17] B. Ding, Z. Liu, D. Seweryniak, P. J. Woods, H. L. Wang, J. Yang, H. L. Liu, C. N. Davids, M. P. Carpenter, T. Davinson, R. V. F. Janssens, R. D. Page, A. P. Robinson, J. Shergur, S. Sinha, S. Zhu, X. D. Tang, J. G. Wang, T. H. Huang, W. Q. Zhang, M. D. Sun, X. Y. Liu, and H. Y. Lu, First identification of excited states in ^{117}Ba using the recoil-β-delayed proton tagging technique, Phys. Rev. C **95**, 024301 (2017).

[18] I. Ahmad, R. R. Chasman, J. P. Greene, F. G. Kondev, and S. Zhu, Electron capture decay of 58-min $^{229}_{92}$U and levels in $^{229}_{91}$Pa, Phys. Rev. C **92**, 024313 (2015).

[19] W. Reviol, R. V. F. Janssens, S. Frauendorf, D. G. Sarantites, M. P. Carpenter, X. Chen, C. J. Chiara, D. J. Hartley, K. Hauschild, T. Lauritsen, A. Lopez-Martens, M. Montero, O. L. Pechenaya, D. Seweryniak, J. B. Snyder, and S. Zhu, Characterization of octupole-type structures in ^{221}Th, Phys. Rev. C **90**, 044318 (2014).

[20] S. K. Tandel, M. Hemalatha, A. Y. Deo, S. B. Patel, R. Palit, T. Trivedi, J. Sethi, S. Saha, D. C. Biswas, and S. Mukhopadhyay, Evolution of octupole collectivity in ^{221}Th, Phys. Rev. C **87**, 034319 (2013).

[21] W. Reviol, D. G. Sarantites, C. J. Chiara, M. Montero, R. V. F. Janssens, M. P. Carpenter, T. L. Khoo, T. Lauritsen, C. J. Lister, D. Seweryniak, S. Zhu, O. L. Pechenaya, and S. G. Frauendorf, Parity doubling in ^{219}Th and the onset of collectivity above *n* = 126, Phys. Rev. C **80**, 011304(R) (2009).

[22] M. Bishof, R. H. Parker, K. G. Bailey, J. P. Greene, R. J. Holt, M. R. Kalita, W. Korsch, N. D. Lemke, Z.-T. Lu, P. Mueller, T. P. O'Connor, J. T. Singh, and M. R. Dietrich, Improved limit on the ^{225}Ra electric dipole moment, Phys. Rev. C **94**, 025501 (2016).

[23] R. H. Parker, M. R. Dietrich, M. R. Kalita, N. D. Lemke, K. G. Bailey, M. Bishof, J. P. Greene, R. J. Holt, W. Korsch, Z.-T. Lu, P. Mueller, T. P. O'Connor, and J. T. Singh, First Measurement of the Atomic Electric Dipole Moment of ^{225}Ra, Phys. Rev. Lett. **114**, 233002 (2015).

[24] J. Dobaczewski and J. Engel, Nuclear Time-Reversal Violation and the Schiff Moment of ^{225}Ra, Phys. Rev. Lett. **94**, 232502 (2005).

[25] N. Auerbach, V. V. Flambaum, and V. Spevak, Collective t-and p-Odd Electromagnetic Moments in Nuclei with Octupole Deformations, Phys. Rev. Lett. **76**, 4316 (1996).

[26] V. V. Flambaum, Enhanced nuclear schiff moment and time-reversal violation in ^{229}Th-containing molecules, Phys. Rev. C **99**, 035501 (2019).

[27] A. V. Afanasjev, H. Abusara, and S. E. Agbemava, Octupole deformation in neutron-rich actinides and superheavy nuclei and the role of nodal structure of single-particle wavefunctions in extremely deformed structures of light nuclei, Phys. Scr. **93**, 034002 (2018).

[28] Y. Fu, H. Wang, L.-J. Wang, and J. M. Yao, Odd-even parity splittings and octupole correlations in neutron-rich ba isotopes, Phys. Rev. C **97**, 024338 (2018).

[29] P. Marević, J.-P. Ebran, E. Khan, T. Nikšić, and D. Vretenar, Quadrupole and octupole collectivity and cluster structures in neon isotopes, Phys. Rev. C **97**, 024334 (2018).

[30] K. Nomura, T. Nikšić, and D. Vretenar, Signatures of octupole correlations in neutron-rich odd-mass barium isotopes, Phys. Rev. C **97**, 024317 (2018).

[31] W. Zhang and Y. F. Niu, Shape transition with temperature of the pear-shaped nuclei in covariant density functional theory, Phys. Rev. C **96**, 054308 (2017).

[32] S. E. Agbemava and A. V. Afanasjev, Octupole deformation in the ground states of even-even *z* ∼ 96, *n* ∼ 196 actinides and superheavy nuclei, Phys. Rev. C **96**, 024301 (2017).

[33] J. M. Yao and J. Engel, Octupole correlations in low-lying states of ^{150}Nd and ^{150}Sm and their impact on neutrinoless double-β decay, Phys. Rev. C **94**, 014306 (2016).

[34] L.-S. Geng, J. Meng, and H. Toki, Reflection asymmetric relativistic mean field approach and its application to the octupole deformed nucleus ^{226}Ra, Chin. Phys. Lett. **24**, 1865 (2007).

[35] J.-Y. Guo, P. Jiao, and X.-Z. Fang, Microscopic description of nuclear shape evolution from spherical to octupole-deformed shapes in relativistic mean-field theory, Phys. Rev. C **82**, 047301 (2010).

[36] L. M. Robledo, M. Baldo, P. Schuck, and X. Viñas, Octupole deformation properties of the Barcelona-Catania-Paris energy density functionals, Phys. Rev. C **81**, 034315 (2010).

[37] L. M. Robledo and G. F. Bertsch, Global systematics of octupole excitations in even-even nuclei, Phys. Rev. C **84**, 054302 (2011).

[38] R. Rodríguez-Guzmán, L. M. Robledo, and P. Sarriguren, Microscopic description of quadrupole-octupole coupling in Sm and Gd isotopes with the Gogny energy density functional, Phys. Rev. C **86**, 034336 (2012).

[39] L. M. Robledo and P. A. Butler, Quadrupole-octupole coupling in the light actinides, Phys. Rev. C **88**, 051302(R) (2013).

[40] R. N. Bernard, L. M. Robledo, and T. R. Rodríguez, Octupole correlations in the ^{144}Ba nucleus described with symmetry-conserving configuration-mixing calculations, Phys. Rev. C **93**, 061302(R) (2016).

[41] L. M. Robledo and G. F. Bertsch, Ground state octupole correlation energy with effective forces, J. Phys. G **42**, 055109 (2015).

[42] J. Zhao, B.-N. Lu, E.-G. Zhao, and S.-G. Zhou, Nonaxial-octupole Y_{32} correlations in $n = 150$ isotones from multidimensional constrained covariant density functional theories, Phys. Rev. C **86**, 057304 (2012).

[43] S.-G. Zhou, Multidimensionally constrained covariant density functional theories—nuclear shapes and potential energy surfaces, Phys. Scr. **91**, 063008 (2016).

[44] K. Nomura, D. Vretenar, and B.-N. Lu, Microscopic analysis of the octupole phase transition in Th isotopes, Phys. Rev. C **88**, 021303(R) (2013).

[45] K. Nomura, D. Vretenar, T. Nikšić, and B.-N. Lu, Microscopic description of octupole shape-phase transitions in light actinide and rare-earth nuclei, Phys. Rev. C **89**, 024312 (2014).

[46] K. Nomura, R. Rodríguez-Guzmán, and L. M. Robledo, Spectroscopy of quadrupole and octupole states in rare-earth nuclei from a gogny force, Phys. Rev. C **92**, 014312 (2015).

[47] S. E. Agbemava, A. V. Afanasjev, and P. Ring, Octupole deformation in the ground states of even-even nuclei: A global analysis within the covariant density functional theory, Phys. Rev. C **93**, 044304 (2016).

[48] J. M. Yao and K. Hagino, Anharmonicity of multi–octupole-phonon excitations in ^{208}Pb: Analysis with multireference covariant density functional theory and subbarrier fusion of ^{16}O + ^{208}Pb, Phys. Rev. C **94**, 011303(R) (2016).

[49] W. Zhang, Z. P. Li, S. Q. Zhang, and J. Meng, Octupole degree of freedom for the critical-point candidate nucleus ^{152}Sm in a reflection-asymmetric relativistic mean-field approach, Phys. Rev. C **81**, 034302 (2010).

[50] Z. Li, B. Song, J. Yao, D. Vretenar, and J. Meng, Simultaneous quadrupole and octupole shape phase transitions in thorium, Phys. Lett. B **726**, 866 (2013).

[51] Z. Li, T. Niksic, and D. Vretenar, Coexistence of nuclear shapes: Self-consistent mean-field and beyond, J. Phys. G **43**, 024005 (2016).

[52] S. Y. Xia, H. Tao, Y. Lu, Z. P. Li, T. Nikšić, and D. Vretenar, Spectroscopy of reflection-asymmetric nuclei with relativistic energy density functionals, Phys. Rev. C **96**, 054303 (2017).

[53] J. M. Yao, E. F. Zhou, and Z. P. Li, Beyond relativistic mean-field approach for nuclear octupole excitations, Phys. Rev. C **92**, 041304(R) (2015).

[54] E. F. Zhou, J. M. Yao, Z. P. Li, J. Meng, and P. Ring, Anatomy of molecular structures in ^{20}Ne, Phys. Lett. B **753**, 227 (2016).

[55] H. Tao, J. Zhao, Z. P. Li, T. Nikšić, and D. Vretenar, Microscopic study of induced fission dynamics of ^{226}Th with covariant energy density functionals, Phys. Rev. C **96**, 024319 (2017).

[56] S. Ebata and T. Nakatsukasa, Octupole deformation in the nuclear chart based on the 3D Skyrme Hartree-Fock plus BCS model, Phys. Scr. **92**, 064005 (2017).

[57] P. Möller, R. Bengtsson, B. G. Carlsson, P. Olivius, T. Ichikawa, H. Sagawa, and A. Iwamoto, Axial and reflection asymmetry of the nuclear ground state, At. Data Nucl. Data Tables **94**, 758 (2008).

[58] H.-L. Wang, J. Yang, M.-L. Liu, and F.-R. Xu, Evolution of ground-state quadrupole and octupole stiffnesses in even-even barium isotopes, Phys. Rev. C **92**, 024303 (2015).

[59] W. Nazarewicz, P. Olanders, I. Ragnarsson, J. Dudek, G. A. Leander, P. Möller, and E. Ruchowsa, Analysis of octupole instability in medium-mass and heavy nuclei, Nucl. Phys. A **429**, 269 (1984).

[60] N. V. Zamfir and D. Kusnezov, Octupole correlations in the transitional actinides and the spdf interacting boson model, Phys. Rev. C **63**, 054306 (2001).

[61] T. Otsuka and M. Sugita, Unified description of quadrupole-octupole collective states in nuclei, Phys. Lett. B **209**, 140 (1988).

[62] A. Dobrowolski, K. Mazurek, and A. Góźdź, Consistent quadrupole-octupole collective model, Phys. Rev. C **94**, 054322 (2016).

[63] N. Minkov, S. Drenska, M. Strecker, W. Scheid, and H. Lenske, Non-yrast nuclear spectra in a model of coherent quadrupole-octupole motion, Phys. Rev. C **85**, 034306 (2012).

[64] R. V. Jolos, P. von Brentano, and J. Jolie, Second order phase transitions from octupole-nondeformed to octupole-deformed shape in the alternating parity bands of nuclei around ^{240}Pu based on data, Phys. Rev. C **86**, 024319 (2012).

[65] P. G. Bizzeti and A. M. Bizzeti-Sona, Octupole transitions in the critical-point nucleus ^{224}Ra, Phys. Rev. C **88**, 011305(R) (2013).

[66] D. Bonatsos, D. Lenis, N. Minkov, D. Petrellis, and P. Yotov, Analytic description of critical-point actinides in a transition from octupole deformation to octupole vibrations, Phys. Rev. C **71**, 064309 (2005).

[67] P. G. Bizzeti and A. M. Bizzeti-Sona, Description of nuclear octupole and quadrupole deformation close to the axial symmetry and phase transitions in the octupole mode, Phys. Rev. C **70**, 064319 (2004).

[68] Y. S. Chen and Z. C. Gao, Reflection asymmetric shell model for octupole-deformed nuclei, Phys. Rev. C **63**, 014314 (2000).

[69] G. Leander and R. Sheline, Intrinsic reflection asymmetry in odd-*A* nuclei, Nucl. Phys. A **413**, 375 (1984).

[70] G. Leander, W. Nazarewicz, P. Olanders, I. Ragnarsson, and J. Dudek, A new region of intrinsic reflection asymmetry in nuclei around ^{145}Ba? Phys. Lett. B **152**, 284 (1985).

[71] G. A. Leander and Y. S. Chen, Rigid reflection-asymmetric rotor description of the nucleus ^{227}Ac, Phys. Rev. C **35**, 1145 (1987).

[72] G. A. Leander and Y. S. Chen, Reflection-asymmetric rotor model of odd $A \sim 219$–229 nuclei, Phys. Rev. C **37**, 2744 (1988).

[73] N. Minkov, S. Drenska, P. Yotov, S. Lalkovski, D. Bonatsos, and W. Scheid, Coherent quadrupole-octupole modes and split parity-doublet spectra in odd-*A* nuclei, Phys. Rev. C **76**, 034324 (2007).

[74] N. Minkov and A. Pálffy, Reduced Transition Probabilities for the Gamma Decay of the 7.8 eV Isomer in ^{229}Th, Phys. Rev. Lett. **118**, 212501 (2017).

[75] Y. Wang, S. Zhang, P. Zhao, and J. Meng, Multiple chiral doublet bands with octupole correlations in reflection-asymmetric triaxial particle rotor model, Phys. Lett. B **792**, 454 (2019).

[76] G. G. Adamian, N. V. Antonenko, R. V. Jolos, and T. M. Shneidman, Cluster interpretation of parity doublet rotational bands in odd-mass nuclei, Phys. Rev. C **70**, 064318 (2004).

[77] Y.-J. Chen, Z.-C. Gao, Y.-S. Chen, and Y. Tu, Octupole bands and simplex inversion in the neutron-rich nucleus ^{145}Ba, Phys. Rev. C **91**, 014317 (2015).

[78] C. Alonso, J. Arias, A. Frank, H. Sofia, S. Lenzi, and A. Vitturi, Description of octupole-deformed nuclei within the interacting boson and interacting boson-fermion models, Nucl. Phys. A **586**, 100 (1995).

[79] M. Bender, P.-H. Heenen, and P.-G. Reinhard, Self-consistent mean-field models for nuclear structure, Rev. Mod. Phys. **75**, 121 (2003).

[80] D. Vretenar, A. V. Afanasjev, G. A. Lalazissis, and P. Ring, Relativistic Hartree-Bogoliubov theory: Static and dynamic aspects of exotic nuclear structure, Phys. Rep. **409**, 101 (2005).

[81] J. Meng, H. Toki, S. Zhou, S. Zhang, W. Long, and L. Geng, Relativistic continuum Hartree-Bogoliubov theory for ground-state properties of exotic nuclei, Prog. Part. Nucl. Phys. **57**, 470 (2006).

[82] J. Stone and P.-G. Reinhard, The Skyrme interaction in finite nuclei and nuclear matter, Prog. Part. Nucl. Phys. **58**, 587 (2007).

[83] T. Nikšić, D. Vretenar, and P. Ring, Relativistic nuclear energy density functionals: Mean-field and beyond, Prog. Part. Nucl. Phys. **66**, 519 (2011).

[84] *Relativistic Density Functional for Nuclear Structure*, edited by J. Meng (World Scientific, Singapore, 2016).

[85] L. M. Robledo, T. R. Rodríguez, and R. R. Rodríguez-Guzmán, Mean field and beyond description of nuclear structure with the Gogny force: A review, J. Phys. G: Nucl. Part. Phys. **46**, 013001 (2018).

[86] P. W. Zhao, S. Q. Zhang, J. Peng, H. Z. Liang, P. Ring, and J. Meng, Novel structure for magnetic rotation bands in ^{60}Ni, Phys. Lett. B **699**, 181 (2011).

[87] P. W. Zhao, J. Peng, H. Z. Liang, P. Ring, and J. Meng, Antimagnetic Rotation Band in Nuclei: A Microscopic Description, Phys. Rev. Lett. **107**, 122501 (2011).

[88] Z. Niu, Y. Niu, H. Liang, W. Long, T. Nikšić, D. Vretenar, and J. Meng, β-decay half-lives of neutron-rich nuclei and matter flow in the r-process, Phys. Lett. B **723**, 172 (2013).

[89] Z. M. Niu, Y. F. Niu, Q. Liu, H. Z. Liang, and J. Y. Guo, Nuclear β^+/EC decays in covariant density functional theory and the impact of isoscalar proton-neutron pairing, Phys. Rev. C **87**, 051303(R) (2013).

[90] S. Quan, Q. Chen, Z. P. Li, T. Nikšić, and D. Vretenar, Global analysis of quadrupole shape invariants based on covariant energy density functionals, Phys. Rev. C **95**, 054321 (2017).

[91] K. Q. Lu, Z. X. Li, Z. P. Li, J. M. Yao, and J. Meng, Global study of beyond-mean-field correlation energies in covariant energy density functional theory using a collective Hamiltonian method, Phys. Rev. C **91**, 027304 (2015).

[92] P. Zhao and Z. Li, Spectroscopies of rod- and pear-shaped nuclei in covariant density functional theory, Int. J. Mod. Phys. E **27**, 1830007 (2018).

[93] B. Bally, B. Avez, M. Bender, and P.-H. Heenen, Beyond Mean-Field Calculations for Odd-Mass Nuclei, Phys. Rev. Lett. **113**, 162501 (2014).

[94] M. Borrajo and J. L. Egido, Symmetry conserving configuration mixing description of odd mass nuclei, Phys. Rev. C **98**, 044317 (2018).

[95] M. Borrajo and J. L. Egido, Ground-state properties of even and odd magnesium isotopes in a symmetry-conserving approach, Phys. Lett. B **764**, 328 (2017).

[96] K. Nomura, T. Nikšić, and D. Vretenar, Beyond-mean-field boson-fermion model for odd-mass nuclei, Phys. Rev. C **93**, 054305 (2016).

[97] S. Quan, W. P. Liu, Z. P. Li, and M. S. Smith, Microscopic core-quasiparticle coupling model for spectroscopy of odd-mass nuclei, Phys. Rev. C **96**, 054309 (2017).

[98] Z. Xu and Z.-P. Li, Microscopic analysis of octupole shape transitions in neutron-rich actinides with relativistic energy density functional, Chin. Phys. C **41**, 124107 (2017).

[99] S. Quan, Z. P. Li, D. Vretenar, and J. Meng, Nuclear quantum shape-phase transitions in odd-mass systems, Phys. Rev. C **97**, 031301(R) (2018).

[100] A. Klein, P. Protopapas, S. G. Rohoziński, and K. Starosta, Kerman-Klein-Dönau-Frauendorf model for odd-odd nuclei: Formal theory, Phys. Rev. C **69**, 034338 (2004).

[101] S. Frauendorf and F. Dönau, Transverse wobbling: A collective mode in odd-A triaxial nuclei, Phys. Rev. C **89**, 014322 (2014).

[102] P. W. Zhao, Z. P. Li, J. M. Yao, and J. Meng, New parametrization for the nuclear covariant energy density functional with a point-coupling interaction, Phys. Rev. C **82**, 054319 (2010).

[103] Y. Tian, Z. Ma, and P. Ring, A finite range pairing force for density functional theory in superfluid nuclei, Phys. Lett. B **676**, 44 (2009).

[104] B. N. Laboratory, National nuclear data center, http://www.nndc.bnl.gov/

[105] T. Nikšić, D. Vretenar, and P. Ring, Relativistic nuclear energy density functionals: Adjusting parameters to binding energies, Phys. Rev. C **78**, 034318 (2008).

[106] P. Protopapas and A. Klein, Possible solution of the coriolis attenuation problem, Phys. Rev. C **55**, 1810 (1997).

[107] See Supplemental Material at http://link.aps.org/supplemental/10.1103/PhysRevC.100.044319 for the calculated intraband and interband $B(E2)$ values and interband $B(E1)$ and $B(E3)$ values of ^{223,225,227}Ra.